Vietnam Journal of Science and Technology ***64*** *(x) (2026)*

doi:10.15625/2525-2518/22041

Concept and optimization of SMA dampers to control the first three natural vibration modes in cable-stayed bridges

Hoang Ngoc Quy[1, 2], Nguyen Van Duy[2], TruongGiang Nguyen[1, 3, *]

[1]*Institute of Mechanics, Vietnam Academy of Science and Technology, 18 Hoang Quoc Viet, Nghia Do, Ha Noi, Viet Nam*

[2]*Faculty of Civil Engineering, VNU University of Engineering and Technology, 144 Xuan Thuy, Cau Giay, Ha Noi, Viet Nam*

[3]*Faculty of Engineering Mechanics and Automation, VNU University of Engineering and Technology, 144 Xuan Thuy, Cau Giay, Ha Noi, Viet Nam*

[*]Emails: *ntgiang@imech.vast.vn*

Received: 5 December 2024; Accepted for publication: 16 June 2025

Abstract. Cable-stayed bridges are often subjected to cable vibrations caused by wind, traffic, and other dynamic loads, which can significantly reduce their structural lifespan. To address this issue, our study proposes a two-floor damping design that leverages the superelasticity and superior energy dissipation capabilities of shape memory alloys (SMA). A simplified constitutive model was developed to simulate the superelastic behavior of SMA, optimizing critical parameters such as length, diameter, and installation position on cable-stayed bridges. Through simulations and dynamic response analysis, the SMA damper demonstrated exceptional effectiveness in dissipating energy across various vibration modes, significantly enhancing structural stability. Furthermore, this paper highlights the advantages of the two-floor SMA damper in mitigating cable vibrations under diverse oscillation modes and identifies an optimal set of parameters for practical installation, contributing to cost efficiency and extended bridge lifespan. A comparison with Tuned Mass Damper (TMD) results is also carried out to evaluate the damping efficiency of the SMA device.

Keywords: Shape memory alloy, Martensitic phase transformation, Superelastic, Vibration, Damper.

Classification numbers: 5.4.5

1. INTRODUCTION

Cable-stayed bridges are a popular choice in modern engineering due to their aesthetic appeal, long spans, and construction efficiency. However, these bridges often experience significant vibrations in the cables caused by wind, traffic, and other dynamic loads, leading to structural fatigue and reduced lifespan [1, 2]. Traditional methods to mitigate these vibrations

typically use passive devices such as tuned mass dampers, friction dampers, viscous dampers, and fluid-based damping systems [3, 4]. While these methods provide some benefits, they also have certain limitations, such as limited damping capacity and maintenance challenges [5].

In recent years, shape memory alloys have emerged as a potential solution for vibration control due to their unique superelastic properties and ability to absorb and dissipate energy. SMA materials, particularly Nickel-Titanium (NiTi) alloys, exhibit significant hysteresis and can withstand large deformations while returning to their original shape, making them ideal for damping applications [6-9]. Research has shown that using SMAs in damping systems can significantly improve the performance of cable-stayed bridges, reducing harmful vibrations and extending the bridge's lifespan [10, 11]. One of the main advantages of SMAs is their exceptional flexibility, allowing them to function effectively in a wide range of environmental conditions. By adjusting the quantity and/or characteristics of the SMA components, it is possible to optimize their energy dissipation capabilities, thereby enhancing damping efficiency. Furthermore, SMAs exhibit excellent fatigue resistance under large deformation cycles and ensure high durability and reliability over long periods of use. These properties are particularly important for cable-stayed bridges, where weather conditions can change rapidly and lead to unpredictable dynamic loads [12]. The superelastic properties of SMAs allow them to absorb and dissipate large amounts of energy from vibrations, mitigating negative impacts on the bridge structure [13, 14]. SMA dampers, such as the proposed SMAS-TMD with pre-tensioned SMA helical springs [9], have shown superior vibration reduction capabilities compared to traditional dampers. Additionally, the use of SMA dampers can effectively prevent the common detuning phenomena observed in optimally tuned mass dampers [15].

This paper presents the detailed design, site survey, and performance evaluation of SMA dampers specifically developed for cable-stayed bridges. Key design factors, such as the optimal length and diameter of SMA wires, are analyzed to maximize damping efficiency. A comprehensive site survey is conducted to identify optimal installation locations, ensuring the dampers deliver the highest performance.

To support this, we propose a simulation model for the superelastic behavior of SMA materials, providing a deeper understanding of their operating mechanisms and enabling damper design optimization. The model is advantageous due to its simplicity and the use of straightforward solution algorithms, making it practical for engineering applications. Additionally, this study examines the dynamic response of cable-stayed bridge cables across multiple natural oscillation modes, offering valuable insights into the performance of SMA dampers under varying vibrational conditions.

The organization of the paper is as follows: section 2 describes the design of the two-floor damper based on the superelastic properties of SMA material, ensuring stability and optimal damping performance. Section 3 develops the fundamental equations for a simplified constitutive model of SMA, grounded in thermodynamic principles and stress-strain relationships, while also presenting the dynamic equations for inclined cables with forces from the SMA damper incorporated. In section 4, numerical results are also compared with those of a TMD to assess the performance of the SMA damper. Moreover, this section also investigates focuses on optimizing the area, length, and installation position of the SMA damper, as well as evaluating its damping effectiveness across the cable's natural oscillation modes. Finally, the conclusions are summarized in Section 5.

2. CONCEPT OF SMA DAMPER

In this concept, we aim to present a two-floor SMA damper with high energy dissipation capacity and complete deformation recovery. A central plate is directly connected to the cable-stayed cables, ensuring that the SMA wires operate under alternating tension as the cables vibrate. The SMA wires are arranged at the four corners of a square layout, providing enhanced stability for the device. This damper is specially optimized to reduce vibrations in the cables of cable-stayed bridges by utilizing shape memory alloy wires, known for their unique superelastic properties. These properties enable efficient energy absorption and recovery after repeated cycles of deformation. The prototype of the SMA damper, shown in the Fig 1, consists of three main parts:

Connection System to the Bridge:

This system secures the damper to the bridge structure. The connection ensures that the damper remains stable and can effectively transmit forces from the vibrating cables to the SMA wires.

Central Plate Moving with the Cable-Stayed Cables:

The central plate is designed to move synchronously with the cable-stayed cables. This plate transfers the vibrational forces from the cables to the SMA wires, ensuring efficient energy absorption by the SMA wires.

Connection System to the Cable-Stayed Cables:

This system links the damper directly to the cable-stayed cables. The robust connection allows the damper to absorb and dissipate the vibrational energy transmitted through the cables.

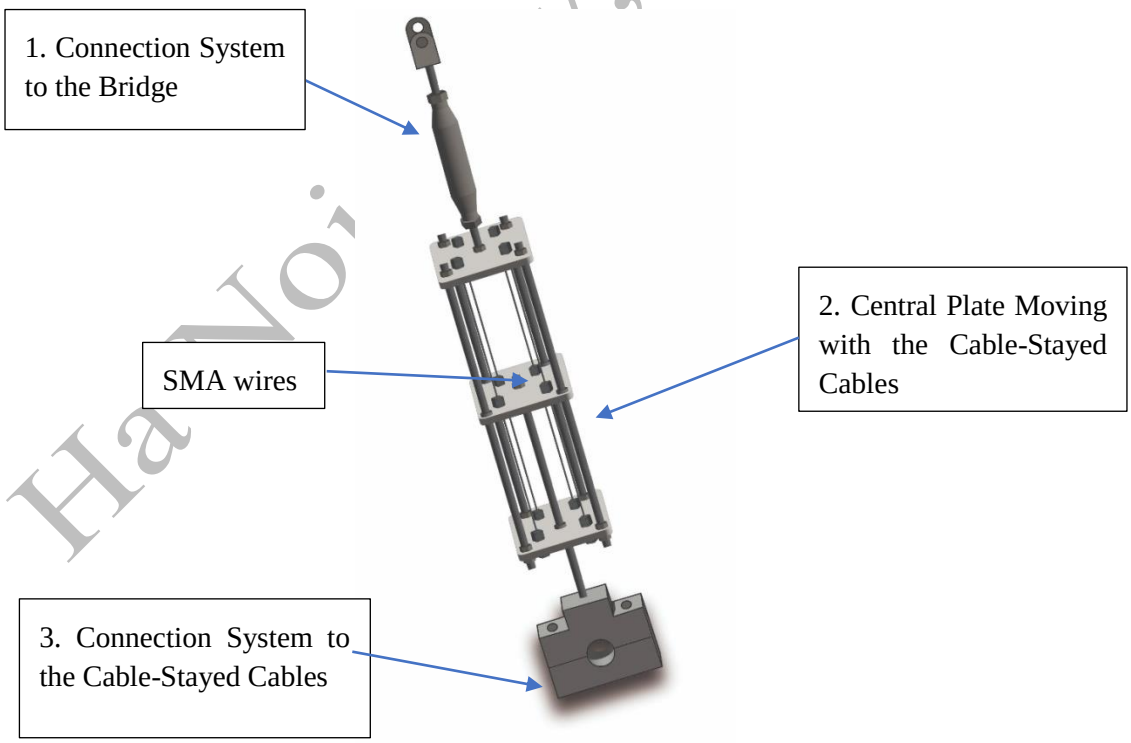

Figure 1. Overall concept of a two-stage damper using shape memory alloy materials.

The SMA wires play a crucial role in the damper, serving as the core component that maximizes the device's energy dissipation efficiency. With a smart concept that incorporates four wires within the structure, the SMA wires are capable of evenly absorbing and distributing vibrational energy. Made from Nickel-Titanium alloy, known for its exceptional strength and fatigue resistance, the SMA wires ensure efficient performance through repeated cycles of mechanical loading and unloading. This concept not only significantly reduces harmful vibrations but also extends the lifespan of cable-stayed bridges. The strategic arrangement and unique shape-memory properties of the SMA wires ensure that the damper operates reliably and stably, making it an ideal solution for vibration control in modern bridge engineering.

3. BASIC EQUATIONS

3.1. Constitutive model for superelastic shape memory alloys

Free energy

In the one-dimensional (1D) model of Shape Memory Alloys, the thermo-mechanical behavior is characterized by a trio of variables: total strain (ε), temperature (T), and the martensite fraction (z). Here, ε represents the deformation experienced by the material, T indicates the operational temperature, and z denotes the proportion of the martensitic phase within the alloy. The martensite fraction z ranges from 0 to 1, where $z = 0$ signifies the material is entirely in the austenitic phase, and $z = 1$ indicates a fully martensitic phase. This modeling approach provides a simplified yet effective means to describe the phase transformation behavior and the corresponding mechanical response of SMAs under various thermal and mechanical loads, facilitating the concept and optimization of SMA-based devices. The Helmholtz free energy density which depends on state variables and internal variables is chosen as:

$$W = W(\varepsilon, T, z) \tag{1}$$

Base on the work by Hoang and Nguyen [16], we propose that the Helmholtz free energy (per unit volume) under isothermal conditions is defined by the following function:

$$W(\varepsilon, \varepsilon^{in}, z) = \frac{1}{2}\left(1 - z + \tau\right)E\left(\varepsilon - \varepsilon^{in}\right)^2 + f(z) \tag{2}$$

where E is constant modulus, τ is a constant and ε^{in} represents the inelastic strain. The hardening function is designed to capture the interactions between the austenitic and martensitic phases, as well as the interactions among the different martensitic variants. This function, $f(z)$, takes the following form during both the forward and reverse phase transformations:

$$f(z) = \begin{cases} \frac{1}{2}Hz^2 + \frac{1}{2}Gz, & \dot{z} > 0 \\ \frac{1}{2}Hz^2 + \frac{1}{2}Iz, & \dot{z} < 0 \end{cases} \tag{3}$$

where H, G, and I are constant material parameters.

Evolution of internal state variables

The Clausius-Duhem inequality can be expressed as:

$$\left(\sigma - \frac{\partial W}{\partial \varepsilon}\right)\dot{\varepsilon} + \left(-\frac{\partial W}{\partial \varepsilon^{in}}\right)\dot{\varepsilon}^{in} + \left(-\frac{\partial W}{\partial z}\right)\dot{z} \geq 0 \tag{4}$$

A sufficient condition for inequality (4) to be satisfied for any $\dot{\varepsilon}$ is that the respective coefficients must be zero, thus yielding:

$$\sigma = \frac{\partial W}{\partial \varepsilon} = (1 - z + \tau)E(\varepsilon - \varepsilon^{in}) \tag{5}$$

Now that we have identified the set of internal state variables ε^{in} and z, we need to determine the evolution equations for these internal state variables. The Clausius-Planck inequality can be expressed as follows:

$$\left(-\frac{\partial W}{\partial \varepsilon^{in}}\right)\dot{\varepsilon}^{in} + \left(-\frac{\partial W}{\partial \xi}\right)\dot{z} \geq 0 \tag{6}$$

By substituting equation (2) into equation (6), we obtain:

$$(1 - z + \tau)E\left(\varepsilon - \varepsilon^{in}\right)\dot{\varepsilon}^{in} - \left(-\frac{1}{2}E\left(\varepsilon - \varepsilon^{in}\right)^2 + \frac{\partial f(z)}{\partial z}\right)\dot{z} \geq 0 \tag{7}$$

The inelastic strain, ε^{in}, depends on the martensite fraction z [17]:

$$\varepsilon^{in} = \varepsilon_L z sgn(\sigma) \tag{8}$$

ε_L is the maximum residual strain, sgn(•) is the sign function, and σ is the uniaxial stress. From equation (8) and substituting equations (7), we derive:

$$\left(\sigma\varepsilon_L sgn(\sigma) + \frac{1}{2}E(\varepsilon - \varepsilon_L z sgn(\sigma))^2 - \frac{\partial f(z)}{\partial z}\right)\dot{z} = \Phi\dot{z} \geq 0 \tag{9}$$

where Φ is defined as above and represents the general thermodynamic force conjugate to z. For the Helmholtz free energy by equation (2), the explicit form of Φ is:

$$\Phi(\varepsilon, z) = \sigma\varepsilon_L sgn(\sigma) + \frac{1}{2}E(\varepsilon - \varepsilon_L z sgn(\sigma))^2 - \frac{\partial f(z)}{\partial z}, \tag{10}$$

we consider uniaxial tension so $sgn(\sigma) = +1$. To complete the model, the rate-independent dissipation potential is formulated as follows:

$$D(\dot{z}) = \Phi_c\dot{z} \text{ with } \Phi_c > 0. \tag{11}$$

It is necessary to establish the conditions under which martensitic phase transformations, both forward and reverse, occur. The constitutive model provided posits that these transformations happen when the thermodynamic force Φ attains a critical threshold. This assumption must be incorporated to ensure that the Clausius-Planck inequality holds true for all potential thermomechanical trajectories.

When the forward martensitic transformation occurs, ż takes positive values because austenite is transforming into martensite. Hence, for the Clausius-Planck inequality (9) to hold, Φ must be positive. Thus, during the forward transformation $\dot{z} > 0$, the function Φ reaches the threshold value:

$$\Phi = \frac{\partial D(\dot{z})}{\partial \dot{z}} = \Phi_c \tag{12}$$

where

$$\Phi_c = \sigma_s^{AM}\varepsilon_L \tag{13}$$

and σ_s^{AM} is the stress that starts the phase transformation from austenite to martensite.

Conversely, during the reverse martensitic transformation, $\dot{z}$ is negative as martensite reverts to austenite. For the Clausius-Planck inequality (9) to be satisfied, Φ must be negative. Therefore, during the reverse transformation $\dot{z} < 0$, the function Φ becomes:

$$\Phi = -\frac{\partial D(\dot{z})}{\partial \dot{z}} = -\Phi_c. \tag{14}$$

where

$$\Phi_c = \sigma_s^{MA}\varepsilon_L \tag{15}$$

and σ_s^{MA} is the stress that starts the phase transformation from martensite to austenite. Finally, when the SMA is in a state where no phase transformation occurs, $\dot{z} = 0$, meaning z remains constant. In this scenario, the Clausius-Planck inequality is automatically satisfied because $\Phi\dot{z} = 0$. The criteria for both forward and reverse martensitic transformations can be encapsulated by introducing a transformation function $f(\varepsilon, z)$, such that:

$$\begin{cases} f(\varepsilon,z) = \Phi - \Phi_c \le 0; & f(\varepsilon,z)\dot{z} = 0; \quad \text{whenever } \dot{z} \ge 0 \\ f(\varepsilon,z) = -\Phi - \Phi_c \le 0; & f(\varepsilon,z)\dot{z} = 0\,; \quad \text{whenever } \dot{z} \le 0. \end{cases} \tag{16}$$

Substituting relation (10) into equations (16) results in two quadratic equations:

$$A_1 z^2 + B_1 z + C_1 = 0 \quad \text{whenever } \dot{z} > 0 \tag{17}$$

$$A_2 z^2 + B_2 z + C_2 = 0 \quad \text{whenever } \dot{z} < 0 \tag{18}$$

The coefficients for these quadratic equations are determined as follows:

$$A_1 = \frac{3}{2}E\varepsilon_L^2 \tag{19}$$

$$B_1 = -H - E\varepsilon_L^2 - 2E\varepsilon_L\varepsilon - E\varepsilon_L^2\tau \tag{20}$$

$$C_1 = \frac{1}{2}E\varepsilon^2 + \varepsilon(E\varepsilon_L + E\varepsilon_L\tau) - \sigma_s^{AM}\varepsilon_L - \frac{G}{2} \tag{21}$$

$$A_2 = \frac{3}{2}E\varepsilon_L^2 \tag{22}$$

$$B_2 = -H - L\varepsilon_L^2 - 2E\varepsilon_L\varepsilon - E\varepsilon_L^2\tau \tag{23}$$

$$C_2 = \frac{1}{2}E\varepsilon^2 + \varepsilon(E\varepsilon_L + E\varepsilon_L\tau) - \sigma_s^{MA}\varepsilon_L - \frac{I}{2}. \tag{24}$$

The solutions can be found by solving quadratic equations (17) and (18).

3.2. Dynamic equations formulation of a sag stay cable

We begin by examining a cable connecting two points, A and B, separated by a distance L and forming an angle θ with the horizontal axis. Considering only the cable's self-weight, this structure remains stable in the plane, with the orthogonal reference system in this plane denoted as Axy. In this plane, the cable can oscillate along the Oy direction (Figure 2a), while out-of-plane oscillations occur along the Az direction, forming the orthogonal frame $Axyz$ [18, 19]. The cable's free vibration modes include the first, second, and third modes, illustrated in Figure

2b. The SMA damper, installed at position xc, generates a force f_c applied to the cable, helping to control and reduce vibrations under various load conditions.

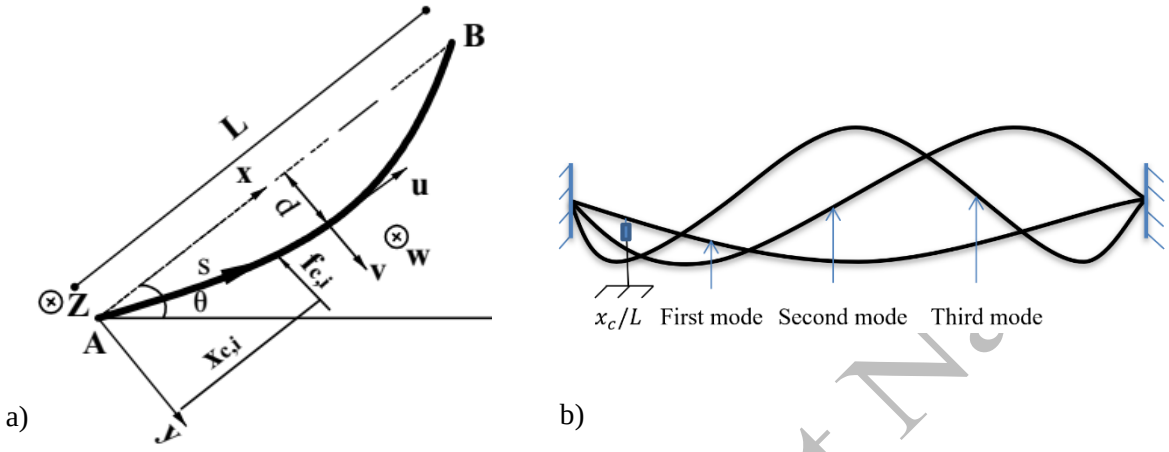

a) b)

Figure 2. a) Schematic diagram of an inclined stay cable and b) Vibration modes of the cable

The partial differential equations governing this equilibrium, while accounting for the influence of an SMA damper, can be expressed as follows [20]:

$$\begin{cases} \dfrac{\partial}{\partial s}\left[(T+\tau)\left(\dfrac{dx}{ds}+\dfrac{\partial u}{\partial s}\right)\right]+F_x(x,t)=m\dfrac{\partial^2 u}{\partial t^2}-mg\sin\theta \\ \dfrac{\partial}{\partial s}\left[(T+\tau)\left(\dfrac{dy}{ds}+\dfrac{\partial v}{\partial s}\right)\right]+F_y(x,t)-\sum_{i=1}^{M} f_{c,i}(t)\,\delta\left(x-x_{c,i}\right)=m\dfrac{\partial^2 v}{\partial t^2}-mg\cos\theta \\ \dfrac{\partial}{\partial s}\left[(T+\tau)\dfrac{\partial w}{\partial s}\right]+F_z(x,t)=m\dfrac{\partial^2 w}{\partial t^2} \end{cases} \quad (25)$$

Where T is the static cable tension, τ is is the dynamic cable tension, t is time, δ is the Dirac delta function, and u, v, w are the displacement components of the cable in the x, y and z directions, respectively, measured from the equilibrium position of the static cable. F_x, F_y and F_z are the distributed dynamic external loads per unit length in the x, y and z directions, and $f_{c,i}$ represents the force exerted by the damper on the cable at position $x_{c,i}$. The Dirac delta function $\delta(x-x_{c,i})$ is used to model the pointwise application of damper forces. The parameter M indicates the total number of SMA dampers installed along the cable. This formulation is consistent with previous studies on coupled dynamic systems with discrete nonlinear damping mechanisms.

To derive the governing equation, the original non-linear equations are simplified using the following key assumptions: the cable's transverse frequency is lower than its longitudinal frequency, vibrations are limited to the xy-plane with negligible movement in the x-direction, the static cable shape is approximated as a parabola, and the sag-to-span ratio is small enough to be ignored. These assumptions were proposed in the research by Soltane et al [21]. The study focuses on the free vibration response of the cable, as initial impulses from wind-induced excitations lead to natural mode vibrations.

As the analysis is restricted to transverse vibrations, we retain only the second equation from the equilibrium system (25), which governs the displacement component v in the y-direction. The transverse deflection can be represented by a finite sum of modes, expressed as:

$$v = \sum_{i=1}^{N} \alpha_i(t)\varphi_i(x) \tag{26}$$

Here, $\alpha_i(t)$ represents the dimensionless mode coefficients, and $\varphi_i(x)$ is a set of mode shape functions assumed to be continuous and satisfying the geometric boundary conditions $\varphi_i(0) = \varphi_i(L) = 0$. To calculate the damping effectiveness of the SMA damper, we assume $\varphi_i(x) = sin\left(\frac{i\pi x}{L}\right)$ with i is the mode number. Based on the assumptions in reference [21], we focus on the second equation in system (25), which governs the transverse vibration in the y-direction and includes the localized forces exerted by the SMA dampers. By multiplying both sides of the equation by $\varphi_j(x)$ and integrating over the length of the cable from 0 to L, we obtain a general form equation:

$$\int_0^L m\frac{\partial^2 v}{\partial t^2}\varphi_j(x)dx - \int_0^L T\frac{\partial^2 v}{x^2}\varphi_j(x)dx + \lambda^2 \int_0^L \int_0^L v(x,t)\varphi_j(x)dx = \int_0^L \left(F_y(x,t) - \sum_{i=1}^{M} f_{c,i}(t)\,\delta(x - x_{c,i})\right)\varphi_j(x)dx \tag{27}$$

Substituting Equation (26) into Equation (27), we obtain:

$$\sum_{i=1}^{N}\left[m\ddot{\alpha}_i(t)\int_0^L \varphi_i(x)\,\varphi_j(x)dx - T\alpha_i(t)\int_0^L \varphi_i''(x)\,\varphi_j(x)dx + \lambda^2\alpha_i(t)\int_0^L \varphi_i(x)dx\int_0^L \varphi_j(x)dx\right] = \int_0^L \left(F_y(x,t) - \sum_{i=1}^{M} f_{c,i}(t)\,\delta(x - x_{c,i})\right)\varphi_j(x)dx \tag{28}$$

Due to orthogonality, the inner products $\int_0^L \varphi_i(x)\,\varphi_j(x)$ and $\int_0^L \varphi_i''(x)\,\varphi_i(x)$ vanish for $i \neq j$, resulting in a decoupled equation for each mode i. After simplification, we obtain:

$$m\ddot{\alpha}_i(t)\int_0^L \varphi_i(x)\,\varphi_i(x)dx - T\alpha_i(t)\int_0^L \varphi_i''(x)\,\varphi_i(x)dx + \lambda^2\alpha_i(t)\int_0^L \varphi_i(x)dx\int_0^L \varphi_i(x)dx = F_{yi} - f_c(t)\varphi_i(x_c) \tag{29}$$

This expression is then simplified by integrating by parts and applying the boundary conditions. Consequently, the modal coefficients $\alpha_i(t)$ must satisfy the following second-order differential equation:

$$m_{ii}\ddot{\alpha}_i(t) + k_{ii}\alpha_i(t) = F_{yi} - f_c(t)\varphi_i(x_c) \tag{30}$$

where:

$$\begin{cases} \lambda^2 = \dfrac{EA}{L}\left(\dfrac{mgcos\theta}{T}\right)^2 \\ m_{ii} = m\displaystyle\int_0^L \varphi_i(x)\varphi_i(x)\,dx = m\frac{L}{2} \\ k_{ii} = -T\displaystyle\int_0^L \varphi_i''(x)\varphi_i(x)dx + \lambda^2\int_0^L \varphi_i(x)dx\int_0^L \varphi_i(x)dx = \dfrac{T\pi^2 i^2}{2L} + \lambda^2\dfrac{4L^2}{i^2\pi^2} \\ F_{yi} = \displaystyle\int_0^L F_y(x,t)\varphi_i(x)dx \\ \varphi_i(x_c) = sin\left(\dfrac{i\pi x_c}{L}\right). \end{cases} \tag{31}$$

Equation (30) captures the essential dynamics of the system, including the mass, stiffness, and damping effects of the cable, as well as the external forces and the influence of the SMA damper. The system of dynamical equations is decoupled in all terms except for the term f_c, which is introduced by the presence of the SMA damper. This SMA damper introduces non-linearity into the otherwise linear cable-damper system. To compute the dynamic response of the cable, the Newmark numerical method is used. The damping force f_c will clearly depend on the constitutive behavior of the SMA.

4. OPTIMIZATION OF THE CROSS-SECTIONAL AREA, LENGTH OF SMA WIRES, AND POSITION OF THE SMA DAMPER

To determine the optimal parameters for the Shape Memory Alloy (SMA), such as the cross-sectional area and the length of the wires, a range of criteria can be applied to ensure maximum efficiency. One of the most widely adopted and effective design approaches involves the use of energy methods [18, 21]. The fundamental principle behind this method is that the SMA reaches its optimal performance when it is capable of dissipating the maximum possible amount of the total energy within the structure. By focusing on energy dissipation, this approach ensures that the SMA can effectively reduce vibrations and enhance structural stability. The energy balance of the equilibrium equation (30) for a single mode can be defined as follows:

$$E_k(t) + E_e(t) = E_i(t) + E_c(t) \tag{32}$$

Where $E_k(t) = \frac{1}{2}m_{ii}\dot{\alpha}_i^2(t)$ is the kinetic energy of the stay cable, $E_e(t) = \frac{1}{2}k_{ii}\alpha_i^2(t)$ is the elastic energy of the stay cable, $E_i(t) = \int_0^t F_{yi}(t)\dot{\alpha}_i(t)\,dt$ is the input energy, and $E_c(t) = E_{ec}(t) + E_{dc}(t)$ is the energy associated with the SMA device, which is a combination of two terms: the elastic energy $E_{ec}(t)$ and the dissipative energy $E_{dc}(t)$. The elastic energy $E_{ec}(t)$ represents the energy stored in the SMA due to its deformation, similar to the elastic energy in the cable. On the other hand, the dissipative energy $E_{dc}(t)$ is related to the energy lost in the system due to hysteresis, which is a measure of the energy dissipation capability of the

SMA. The dissipative term is particularly important because it highlights the SMA's ability to absorb and dissipate energy, reducing the oscillations and enhancing the stability of the structure. To maximize the damping capacity, the dissipative energy must be at its maximum, which results in the maximum force exerted by the SMA. The force exerted by the SMA is as follows:

$$f_c(t) = E\pi D_{SMA}^2 \left(\frac{v(x_c,t)}{L_{SMA}} - z\varepsilon_L \text{sgn}(\varepsilon) \right) \tag{33}$$

Here, E is the modulus of elasticity, $v(x_c,t)$ the cable transverse displacement at location x_c, and L_{SMA} and D_{SMA} are the length and the wire radius of SMA, respectively. According to Equation (33), in order for f_c to reach its maximum value, the term inside the parentheses must also be maximized. In that case, $z = 1$, leading to $\varepsilon = \frac{v(x_c,t)}{L_{SMA}} = \varepsilon_{max}$. Therefore, the condition for optimizing the SMA device length is defined by the relationship:

$$\varepsilon_{max} = \varepsilon_f^{AM} \tag{34}$$

where ε_f^{AM} is the strain corresponding to the stress at the end of the martensite transformation. Consequently, the optimal length of the SMA device is determined by:

$$L_{SMA}^{opt} = \frac{|v^{max}(x_c,t)|}{\varepsilon_{max}} \tag{35}$$

Moreover, based on Equation (33), the radius of the SMA wire in the SMA device should be selected as large as possible.

To examine the damping effectiveness of the SMA device in all three natural vibration modes, the geometry and properties of the stay cable are given in Table 1.

Table 1. Geometric and properties of the stay cable model [21]

Parameter	Symbol	value	unit
Cable length	L	55.4	m
Mass per unit length	m	44	Kg/m
Inclination angle	θ	16.5	deg
Elastic modulus	E_c	19e10	N/m^2
Cross-sectional area	A_c	55.5e-4	m^2
Static tension	T	4313.5e3	N

The formula commonly used to calculate the deflection of a stay cable is: $d = \frac{mgL^2 \cos\theta}{8T}$

In the case of the Rades-La Goulette cable-stayed bridge [21], the tension in the stay cable is $T = 4313kN$, which results in a deflection of $d = 0.043m$. It is clear that when the cable is fitted with a damper, its oscillation amplitude is reduced compared to when it is not equipped. Thus, $d > v^{max}$. To calculate the optimal length of the SMA damper, we fixed the installation position of the damper at $0.1L$. The strain ε_f^{AM} and the material properties of the SMA are provided in Table 2. The maximum transverse displacement $v^{max}(x_c,t)$ is selected as $0.03\ m$, ensuring it is less than the transverse displacement at the mid-span of the cable. The diameter of the SMA wire is chosen to be $D_{SMA} = 20\ mm$. Based on these parameters, the optimal length of the SMA is determined using Equation (35) to be $L_{SMA}^{opt} = 0.46$ m.

Table 2. Material parameters [22].

E_A (Mpa)	E_M (Mpa)	σ_s^{AM} (Mpa)	σ_s^{MA} (Mpa)	E (Mpa)	ε_f^{AM} (%)	τ	H (Mpa)	I (Mpa)	G (Mpa)	ε_L (%)
40000	20000	200	200	20000	6.5	1	7	14	0.2	5

With the above parameters and the calculated optimal length, the damping performance of the SMA device is demonstrated in Figure 3, which presents the dynamic response of the cable under its first three natural vibration modes. Specifically, Figure 3 illustrates the dynamic response of the cable in its first three vibration modes, represented by the transverse displacement $v(x_c, t)$ over time and the corresponding force response f_c as a function of $v(x_c, t)$. The left plot shows the variation of the transverse displacement across the three vibration modes over time. In the first vibration mode, the amplitude decays more slowly than in the second and third modes, indicating higher energy dissipation in the higher modes. Because the frequency of mode 3 exceeds that of mode 2, which in turn surpasses mode 1, faster energy dissipation occurs. This observation is reinforced by the right plot, which depicts the relationship between force f_c and displacement (x_c, t). The first mode has the lowest force, while the second mode, and especially the third mode, exhibit significantly higher forces, suggesting that the SMA damper generates stronger force responses in the higher vibration modes. This reflects the nonlinear characteristics of the SMA damper, where the force response level varies according to each vibration mode.

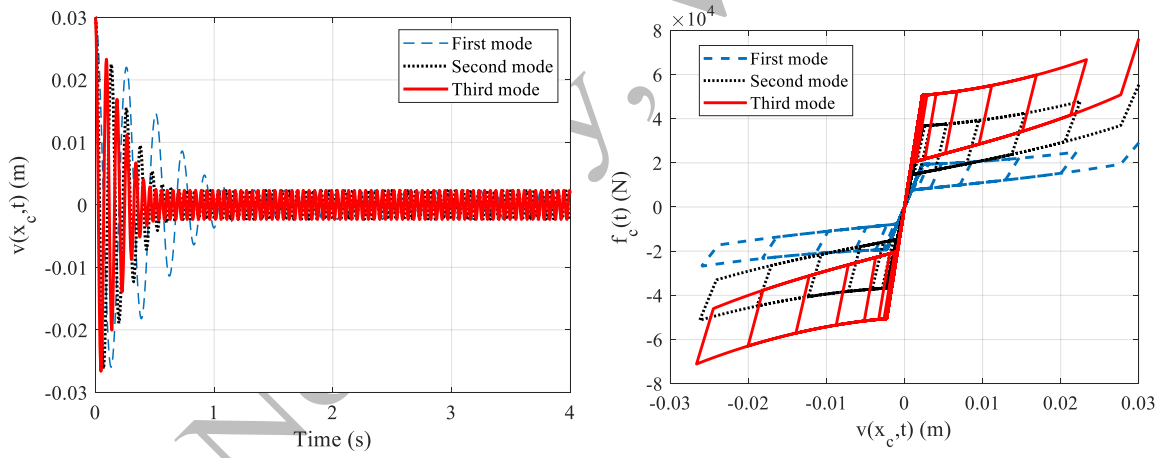

Figure 3. The dynamic response of the cable's three vibration modes

To further emphasize the advantages of the proposed two-floor SMA damper, a comparison is made with the traditional Tuned Mass Damper (TMD), a well established solution for vibration control in cable-stayed bridges. In the study by Mekki [18], the TMD was installed at the mid-span of the cable and optimized using a mass ratio of 5% to target a specific natural mode. The time-history responses, illustrated in Figures 4 to 6, demonstrate that the SMA damper consistently provides faster attenuation of vibration amplitudes and shorter stabilization times across all modes.

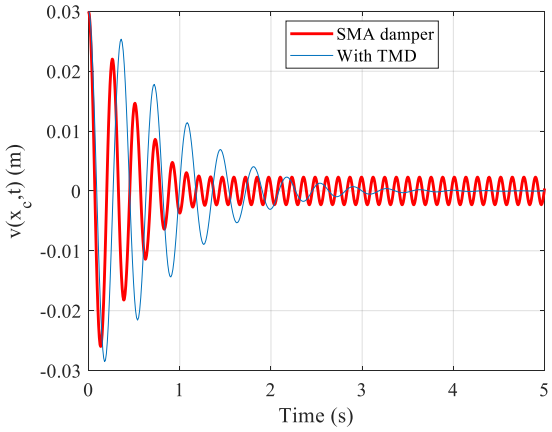

Figure 4. Comparison between the SMA damper and the TMD in controlling the free vibration of the stay cable in the first mode.

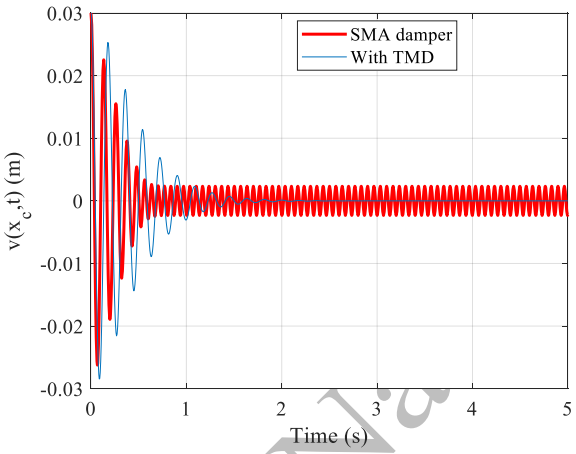

Figure 5. Comparison between the SMA damper and the TMD in controlling the free vibration of the stay cable in the second mode.

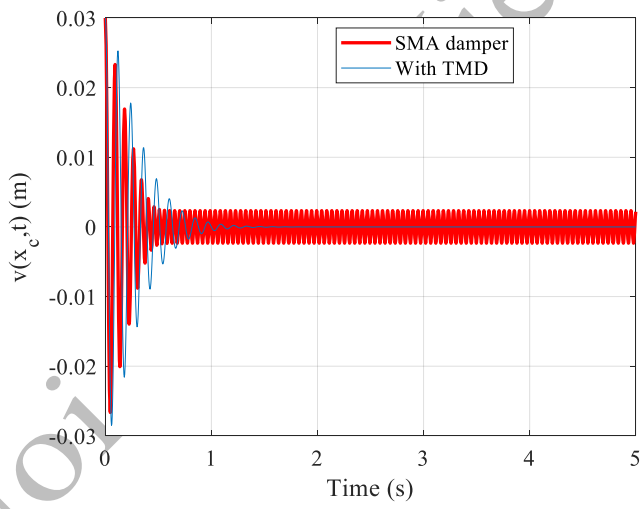

Figure 6. Comparison between the SMA damper and the TMD in controlling the free vibration of the stay cable in the third mode.

Quantitatively, the maximum displacement observed with the SMA damper is reduced by approximately 50 – 60 % compared to the TMD across the modes, and the time to reach stable oscillation is notably shorter. For instance, in the first mode, the SMA-controlled cable stabilizes in under 1.5 seconds, while the TMD requires more time. This indicates a higher effective damping capacity of the SMA, which stems from its intrinsic hysteresis and phase transformation behavior. This trend continues in the higher modes. In the second mode (Figure 5), the SMA damper achieves faster suppression of the oscillation envelope, with a significant reduction in peak amplitude and a quicker transition to steady-state response than the TMD. In the third mode (Figure 6), where the excitation frequency is highest, the SMA damper continues to exhibit superior damping performance, maintaining a compact and stable vibration profile while the TMD response remains more oscillatory and prolonged. One possible advantage of the

TMD under free vibration is its ability to more effectively attenuate small-amplitude oscillations. These results confirm that the proposed SMA damper consistently provides robust vibration control in each individual mode, outperforming the traditional TMD not only in damping intensity but also in response speed and adaptability across different independently examined natural modes.

In addition to evaluating performance, the influence of design parameters on damper efficiency is also examined. The relationship between the SMA diameter, damper installation position, and optimal force f_c is shown in Figure 7.

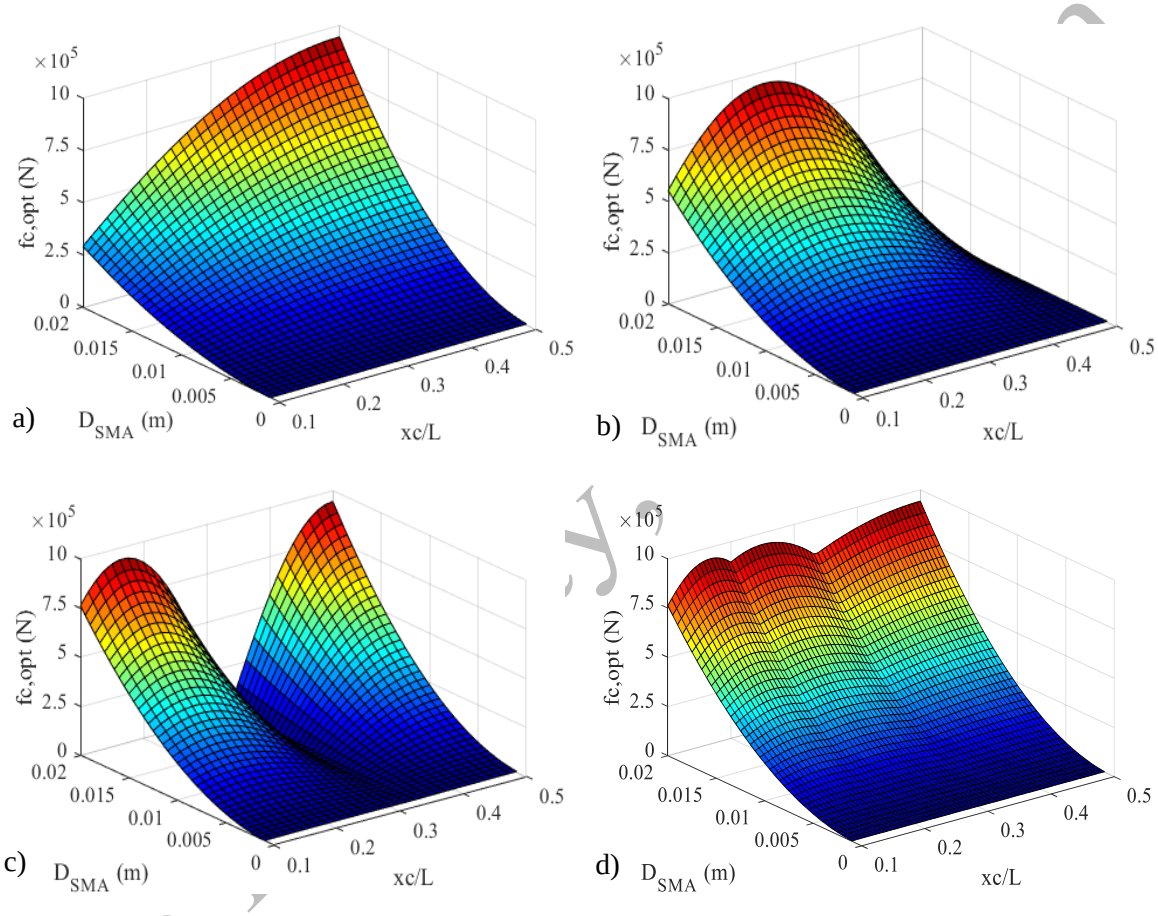

Figure 7. Relationship between diameter, position and force f_c: a) First mode, b) Second mode, c) Third mode and d) Combine three modes.

Figure 7 illustrates the relationship between the SMA diameter (D_{SMA}), the damper installation position (x_c/L), and the optimal force $f_{c,opt}$ across three vibration modes of the cable, along with a combined plot for all three modes. In the first mode (Figure 7a), $f_{c,opt}$ increases significantly as D_{SMA} increases and the installation position moves closer to mid-span, indicating that the best damping effect is achieved when the damper is placed at the mid-span with a larger SMA diameter. For the second mode (Figure 7b), $f_{c,opt}$ also increases with a larger D_{SMA} and reaches optimal damping performance when the damper is installed near a quarter-span position, suggesting that this is the ideal location for the second mode oscillations. In the

third mode (Figure 7c), $f_{c,opt}$ similarly rises with an increasing D_{SMA}, with the best damping effect observed when the damper is installed at either a sixth-span or mid-span position. For each vibration mode, the plots enable engineers to efficiently calculate the optimal damping force required to reduce vibrations in the cable-stayed bridge cables, using the available parameters. The combined plot (Figure 7d) incorporates the effects of all three oscillation modes, showing regions where $f_{c,opt}$ reaches its maximum. This diagram also indicates that the maximum damping force can be easily determined from parameters D_{SMA} and x_c/L to enhance the damper's vibration reduction capability in cases where the cable is subjected to all three vibration modes. This insight is crucial for the practical installation of dampers on stay cables, helping to optimize costs, ensure effective damping, and enhance the longevity of bridge structures.

5. CONCLUSIONS

This study presented a passive two-floor damper based on the superelastic effect of SMA to control vibrations in cable-stayed bridge systems. The two-floor damper was designed to maximize energy dissipation and ensure full deformation recovery after each vibration cycle, thereby enhancing cable stability and extending the service life of the bridge. Additionally, we proposed a simplified constitutive model that accurately simulates the superelastic effect of SMA, meeting the requirements for structural engineering applications. Using this model, we derived the dynamic equations to describe the cable's response when the damper is applied across different natural vibration modes. The results indicate that the two-floor SMA damper achieves high effectiveness in reducing cable oscillation amplitudes, outperforming a conventional tuned mass damper in both peak displacement reduction and stabilization time, particularly in higher vibration modes where energy dissipation is crucial.

We also optimized the length and diameter of the SMA wires to achieve maximum energy dissipation and developed charts illustrating the damping efficiency of the two-floor SMA damper according to installation position and wire diameter across three vibration modes of the cable in cable-stayed bridges. These charts assist in selecting the optimal installation position in practice to ensure high damping efficiency, while also providing feasible design guidance for real-world applications.

The two-floor damper concept with a simplified constitutive model not only optimizes damping performance but also simplifies the design and construction process, ensuring stability and durability for cable-stayed bridges. Future studies can focus on refining the configuration of the two-floor damper to further enhance vibration control, particularly for large bridge systems subjected to complex dynamic loads.

Acknowledgements. This work has been supported by VNU University of Engineering and Technology under project number CN24.22.

CRediT authorship contribution statement. TruongGiang Nguyen: Conceptualisation, Methodology, Review and Supervision. Hoang Ngoc Quy: Investigation, Manuscript Writing and Editing. Nguyen Van Duy: Computing and Editing .

Declaration of competing interest. The authors declare that there is no conflict of interest in this paper.

REFERENCES

1. Xu Y. L., Zhu L. D., Wong K. Y., and Chan K. W. Y. - Field measurement results of Tsing Ma suspension bridge during Typhoon Victor, Structural engineering and mechanics: An International Journal **10** (6) (2000) 545-559.
2. Matsumoto M., Shiraishi N., and Shirato H. - Rain-wind induced vibration of cables of cable-stayed bridges. Journal of wind engineering and industrial aerodynamics **43** (1-3) (1992) 2011-2022.
3. Kareem A., Kline, S. -Performance of multiple mass dampers under random loading. Journal of structural engineering **121** (2) (1995) 348-361
4. Spencer Jr, B. F., Nagarajaiah, S. - State of the art of structural control. Journal of structural engineering **129** (7) (2003) 845-856.
5. Xu Y. L., Xia, Y. - Structural health monitoring of long-span suspension bridges. CRC Press (2011).
6. Liu Y., Van Humbeeck J. - On the damping behaviour of NiTi shape memory alloy. Le Journal de Physique IV **7** (C5) (1997) C5-519.
7. Lagoudas D. C. - Shape memory alloys. Science and Business Media, LLC (2008).
8. Pan Q., Cho C. - Damping property of shape memory alloys. Proceedings of the 17th International Metallurgical and Materials Conference METAL (2008).
9. Lv H., Huang, B. - Parametric study of a new tuned mass damper with pre-strained SMA helical springs for vibration reduction. Smart Structures and Systems **31** (1) (2023) 89-100.
10. DesRoches R., Smith B. - Shape memory alloys in seismic resistant design and retrofit: a critical review of their potential and limitations. Journal of earthquake engineering **8** (3) (2004) 415-429.
11. Rajoriya S., Mishra S. S. - Application of SMA wire in vibration mitigation of bridge stay cable: a state-of-the-art review. Innovative Infrastructure Solutions **7** (3) (2022) 192.
12. Dolce M., Cardone D., Marnetto R. - Implementation and testing of passive control devices based on shape memory alloys. Earthquake engineering & structural dynamics **29** (7) (2000) 945-968.
13. Machado L. G., Savi M. A. - Medical applications of shape memory alloys. Brazilian journal of medical and biological research **36** (2003), 683-691.
14. Helbert G., Dieng L., Chirani S. A., Saint-Sulpice L., Lecompte T., Calloch S., Pilvin P. - Investigation of NiTi based damper effects in bridge cables vibration response: Damping capacity and stiffness changes. Engineering Structures **165** (2018) 184-197.
15. Huang H., Mosalam K. M., Chang W. S. - Adaptive tuned mass damper with shape memory alloy for seismic application. Engineering Structures **223** (2020) 111171.
16. Hoang Ngoc Quy, Haidang Phan, Phan Dinh Hau and TruongGiang Nguyen - Simulation of superelastic behavior of shape memory alloy considering the influence of strain rate. Tuyển tập công trình Hội nghị Cơ học toàn quốc lần thứ XI, Hà Nội (02-03/12/2022) 474-484.
17. Auricchio F., Sacco E. - A one-dimensional model for superelastic shape-memory alloys with different elastic properties between austenite and martensite. International Journal of Non-Linear Mechanics **32** (6) (1997) 1101-1114.
18. Mekki O. B., Auricchio F. - Performance evaluation of shape-memory-alloy superelastic behavior to control a stay cable in cable-stayed bridges. International Journal of Non-Linear Mechanics **46** (2) (2011) 470-477.

19. Rajoriya S., Mishra S. S. - Vibration Mitigation of Stay Cable Using SMA Wire: A Numerical Study. International Symposium on Plasticity and Impact Mechanics. Springer Nature Singapore (2022, August) 205-219.
20. Irvine H. M. - Cable structures the mit press. Cambridge, MA (1981) 15-24.
21. Soltane S., Mekki O. B., Montassar S. - Optimal Design of a Passive SMA Damper to Control Multi-modal Stay Cable Vibrations. Journal of Vibration Engineering & Technologies **11** (3) (2023) 1343-1358.
22. Fugazza D. - Use of shape-memory alloy devices in earthquake engineering: Mechanical properties, advanced constitutive modelling and structural applications. PhD, Univ Degli Stud Di Pavia (2005).